

# Preprocessing of fMR Datasets

Frithjof Kruggel, Xavier Descombes, D. Yves von Cramon  
Max-Planck-Institute of Cognitive Neuroscience  
Inselstraße 22-26, 04103 Leipzig, Germany  
{kruggel,descombe,cramon}@cns.mpg.de

## Abstract

*When studying complex cognitive tasks using functional magnetic resonance (fMR) imaging one often encounters weak signal responses. These weak responses are corrupted by noise and artifacts of various sources. Preprocessing of the raw data before the application of test statistics helps to extract the signal and thus can vastly improve signal detection. We discuss artifact sources and algorithms to handle them. Experiments with simulated and real data underline the usefulness of this preprocessing sequence.*

## 1. Introduction

Many neuronal brain activations elicit an oxygen consumption and give rise to a hemodynamic response of the supplying vascular system. This response is measured as the so-called BOLD (blood-oxygen-level-dependent) effect in fMR imaging. In T2\*-weighted images, this BOLD effect gives rise to an intensity change restricted to a certain brain area and transient in time with respect to the stimulation. However, effects are small and corrupted by noise and artifacts, so that roughly 40-200 repetitions are necessary to detect a statistically significant response.

This high repetition count is especially problematic with complex cognitive tasks like memory or language experiments. Because a test person needs several seconds to complete a single trial, the total time to run an experiment easily adds up to a scanner time of 2 hours which - due to the uncomfortable test situation - is hardly acceptable even for healthy volunteers. With language experiments, such a high number of similar stimuli featuring the same categorical effects and difficulty is hard to find. Thus, one obviously wants to limit the number of repetitions with the help of more sensitive signal detection methods. However, one needs to track the signal-to-noise ratio to delimit the type I error, which corresponds to false positively detected areas.

It is often interesting to compare the test performance between different blocks which are placed several minutes

apart in the experimental design. Scanner instabilities lead to baseline fluctuations with time and often make it impossible to separate functional activation from baseline fluctuations in a statistical analysis. This may be improved by preprocessing the raw data in order to estimate and subtract this baseline before applying any statistical procedure.

There is an increasing interest in the time course (i.e. the shape) of the hemodynamic response and its modulation with respect to different experimental conditions. At the time being, there is no consensus about a physiological model for the neurovascular coupling [29, 4, 24, 11] which would allow to derive a spatio-temporal model function for the hemodynamic response [12, 19, 6, 25]. Thus, the signal restoration corresponds to an ill-defined inverse problem [28]. Instead of modeling a hypothetical signal, we propose to restore the measured spatio-temporal signal. Methods for image restoration are well studied [1, 15, 7, 8] and may be applied in the context of functional neuroimaging.

Research in the processing of fMR time series has concentrated so far on statistical problems (for a review, see [18]) and tried to solve the deconvolution of artifacts and baseline instabilities within a statistical framework [2]. The most widely used method to improve the signal-to-noise ratio is spatial smoothing [22], which obviously lowers the spatial resolution. Prior to statistics, the correction of movement artifacts has been suggested [13]. Various types of artifacts have been identified [21, 27]. Very recently, a "blind deconvolution" technique called "independent component analysis" (ICA), which has been developed for the reconstruction of auditory signal sources, has been applied to fMR data [20].

However, no framework for fMR data preprocessing has been proposed, in which known influences on signal quality are handled by well-established image processing techniques. In this paper, we discuss sources of artifacts in fMR data and how they can be deconvolved. Special attention has been paid to assess the quality of the reconstruction and the parameter optimization with respect to constraints of the experimental design.

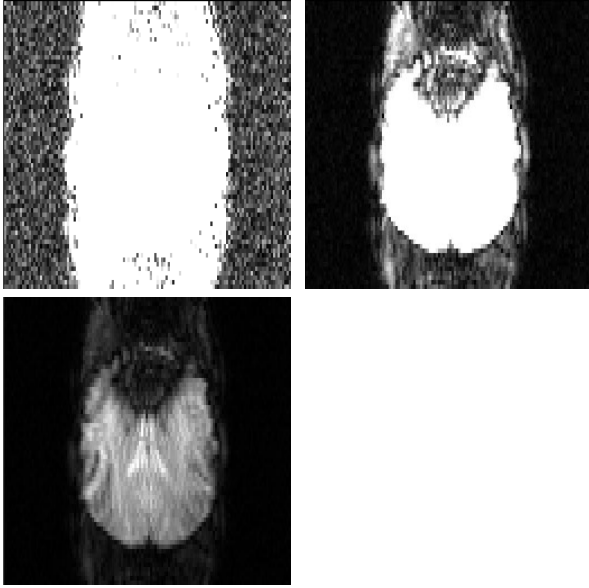


**Figure 1. Example slice from a fMR time series. The histogram of this image was scaled by different factors to enhance various types of artifacts: noise (upper row, left), ghost images (right), signal voids and arc-like artifacts (lower row, left).**

The remainder of this paper is organized as follows: in section 2, we review known artifacts impairing the quality of fMR data, in section 3, we discuss strategies for their restoration, in section 4, experiences and results with simulated and real data are compiled. Finally, we discuss the usefulness of this framework in the context of cognitive fMR neuroimaging studies.

## 2. Artifact Classes

Several sources of artifacts (see Fig. 1) are identifiable: (1) gross body movements during the experimental session, (2) physiological movements (pulsations, swallowing, abdominal movements, breathing), (3) regional sensitivity losses (signal voids) due to susceptibility differences at tissue borders (i.e. the transition bone-brain), (4) ghost images, (5) flow artifacts in the vicinity of large vessels, (6) long-term instabilities of the scanner baseline, (7) noise. An *a posteriori* correction of these artifacts may be accomplished by:

- Aperiodical, small body movements ( $< 2 - 4\text{mm}$ ) are corrected by registration of slices in the time series.
- Timesteps in which gross body movements during the image acquisition phase occur (“blurred slices”) are detected and excluded from further analysis.

- Baseline instabilities of the MR scanner are detectable as slow fluctuations of the mean signal intensity in the time series of a voxel. The baseline may be estimated by low-pass filtering and then subtracted from the original signal. The T2-weighted image is hereby separated from the functional activation.
- Recent fMR studies mostly follow a single- or embedded-single-trial design, which has - in contrast to a block design - a high frequent stimulus periodicity. Using matched bandpass filters, noise and periodic but uncorrelated artifacts (breathing, pulsations) from the functional signal can be separated.

Another option for the correction of gross body movements is given by using navigator echoes or by correction in the k-space [17]. Because such artifacts are encountered in well below 1% of the timesteps their exclusion is not considered a relevant restriction. Regional sensitivity losses and ghost images are handled more efficiently by optimizing the fMR protocols and are not treated in the context of this paper, although in practice, they contribute significantly to data distortions. Furthermore, we do not discuss spatial distortions found with some fMR techniques (most important in *echo planar imaging*) which are attributable to their sensitivity to inhomogeneities of the  $B_1$  magnetic field.

## 3. Algorithms

We propose the preprocessing of raw fMR data by a sequence of 4 steps: (1) artifact detection, (2) movement correction, (3) baseline correction, and (4) signal restoration.

We consider a set of sites  $S \times T = \{(s = (i, j), t)\}$  defined by the time samples for each voxel in the context of fMR signals ( $s$  represents the spatial coordinates and  $t$  the temporal coordinate) and a state space  $\Lambda$  (possible values for the samples). A fMR temporal signal is then an element of the configuration space  $\Omega = \Lambda^{S \times T}$  denoted  $Y = \{y_s(t), t \in T, s \in S\}$ .

Currently, our fMR protocols only allow the acquisition of a set of image slices at a given timestep, i.e. the spatial resolution is much higher within a plane than between planes. There is also a small gap between planes in which no signal is recorded. So we consider slices to be independent and treat two-dimensional spatial models only. All algorithms discussed here are easily extendible to three spatial dimensions. In our models the third dimension corresponds to time. To simplify notations, let us denote an image slice  $I(t_0)$  at timestep  $t_0$  by  $I(t_0) = \{y_s(t_0), s \in S\}$  and a time series  $T(s)$  at voxel  $s = (i, j)$  by  $T(s) = \{y_s(t), t \in T\}$ .

### 3.1. Artifact Detection

A time series of slices is segmented into a mean foreground (brain) and mean background by a k-means classification and subsequent morphological closing. Then for each slice, we compute the mean signal intensity and its variance in the foreground and background region. These four datums are collected and classified for a given slice over the whole time series. Slices at timesteps with gross body movements appear as "blurred images" in the sequence and thus exhibit a lower ratio between foreground and background intensity. Magnetization artifacts occur during the non-equilibrium conditions during sequence startup and are detected as high intensity outliers. The ratio of foreground variance and background variance yields an information about the amount of pulsation artifacts and the contribution of ghost images, more than it reflects the contribution of noise in the data. Outliers are marked for exclusion in the statistical evaluation. These ratios are a crude indicator for the raw data quality and can be reported to the user.

### 3.2. Motion Correction

Small physiological movements ( $< 2 - 4\text{mm}$ ) are corrected by registration of the slices in the time series. Generally, an image slice  $I(t)$  is registered onto a reference  $I(t_0)$  by application of an affine transformation  $A$ :  $I^a(t) = A(I(t))$ . We define a cost function  $C := C(I^a(t), I(t_0))$ , which reflects the likelihood between transformed slice and reference. The likelihood is maximized by modifying the transformation parameters  $A := \text{argmax} C(I^a(t), I(t_0))$ . In this context, we set up a affine transformation consisting of a two translational and a single rotational parameters. The cost function is given by the image cross-correlation [13]:

$$C = \frac{\sum^S (y_s(t) * y_s(t_0))}{\sqrt{\sum^S y_s(t)^2 * \sum^S y_s(t_0)^2}}, \quad (1)$$

which is maximized using the Simplex algorithm [23].

### 3.3. Baseline Estimation

In fMR datasets, slow time-dependent intensity fluctuations are found at any given foreground voxel (see Fig. 4, top left). These fluctuations are dependent on the voxel location (i.e. on the tissue properties), the scanner properties (i.e. linearity, long-term stability), and perhaps also due to physiological variations. These fluctuations often make up to 10% of the signal and thus can easily hide functional activations. We suggest to estimate the baseline and subtract it from the input signal. Here, one has to be cautious not

to model signal changes attributable to functional activation. We restrict to the baseline estimation in the time series only: a spatio-temporal filter needs to track of anatomical edges (i.e. the transition CSF-cortex) and thus requires edge-preserving properties in the spatial domain. With limited testing, we have found no advantage of using spatial information here.

Several options from classical time series analysis are available for baseline estimation: (1) moving average (MA) filters, (2) finite impulse response (FIR) filters, and (3) autoregressive-moving average (ARMA) models. The MA filter estimates the state of a voxel at time  $t_0$  from the mean in a window of  $2N + 1$  time points around  $t_0$ :

$$y_s^f(t_0) = \sum_{r=-N}^N y_s(t_0 + r) / (2N + 1), \quad -N \leq r \leq N. \quad (2)$$

The FIR lowpass filter is given by the following equation [26]:

$$y_s^f(t_0) = \sum_{r=-N}^N \phi_r w_r y_s(t_0 + r), \quad -N \leq r \leq N, \quad (3)$$

where  $\phi_r = \frac{\sin(r\lambda)}{r\pi}$  denote the  $2N + 1$  lowpass filter coefficients for the cut-off frequency  $\lambda$ , and  $w_r$  the  $2N + 1$  coefficients of a Hamming window:

$$w_r = 0.54 + 0.46 \cos\left(\frac{\pi r}{N}\right), \quad -N \leq r \leq N. \quad (4)$$

In the ARMA model, we consider the baseline to be a realisation of the process

$$y_s^f(t) = \sum_{r=1}^p \alpha_r y_s(t - r) + \sum_{r=1}^q \beta_r \epsilon(t - r) + \epsilon(t), \quad (5)$$

where  $\alpha_r$  are the  $p$ , resp.  $\beta_r$  the  $q$  parameters of the ARMA( $p, q$ ) process [30], and  $\epsilon(t) \sim N(0, \sigma^2)$ .

The output of the filter is subtracted from the input signal which effectively results in highpass filtering and likewise separates the anatomical information from the functional activation.

### 3.4. Signal Restoration

At this point in the preprocessing, the signal is composed of (1) the functional activation, (2) uncorrelated signal variations (pulsations, breathing), and (3) noise. In a spectrum of the time series, the functional response due to a stimulus corresponds to a peak in the low-frequency range with all of our current experimental designs (see Fig. 5, top right). Thus, we have studied simple FIR lowpass filters to select a spectral band which only includes the first one or two harmonics of the stimulus frequency. However, such a lowpass

filter requires adaption to the stimulation frequency for a given experimental design. In addition, since the spectral properties of a hemodynamic response are not known, it is *a priori* unclear how many harmonics are to be included in the pass band.

Because the anatomical edges are now absent, we may take advantage of any spatial information to restore the functional signal. The aim of restoration is to add some constraints of homogeneity and smoothness on the solution. A common approach in functional imaging is to use a *spatial* lowpass filter to improve the signal-to-noise ratio. Lowpass filters smooth the data without taking the properties of the underlying signal into account. So high frequency components are lost, i.e. edges in the image are blurred. Using a Markov random field (MRF) as a prior in a Bayesian framework improves the restoration of fine structures and along edges. We do not formally introduce MRFs here [5], but restrict to describe the specifics of the model applied in this context only [9, 10].

We consider that the data  $X$  consists of the underlying signal  $Y$ , corrupted by additive noise  $\eta$ . Reformulating this ill-posed inverse problem in a Bayesian framework, we have to maximize the *a posteriori* probability  $P(Y|X)$ :

$$P(Y|X) = \frac{P(X|Y)P(Y)}{P(X)} \propto P(X|Y)P(Y), \quad (6)$$

where  $P(X|Y)$  refers to the likelihood (or data attachment) and  $P(Y)$  to the prior model.  $P(X|Y)$  is defined by the noise model whereas  $P(Y)$  is defined by the proposed edge preserving MRF. A Gibbs field formulation of the prior probability is given by:

$$\begin{aligned} P(Y) &= \frac{1}{Z} \exp[-U(Y)] \\ &= \frac{1}{Z} \exp[-\sum_{c \in \mathcal{C}} V_c(y_s(t), (s, t) \in c)], \quad (7) \end{aligned}$$

where  $U$  is the energy function,  $\mathcal{C}$  is a finite subset of voxels (a clique),  $V_c$  is the potential associated with the clique  $c$  and  $Z$  a normalization constant.

We consider a 3D spatio-temporal MRF model, where two dimensions correspond to the spatial dimensions of a fMR slice and the third dimension refers to the temporal domain. The 4 next neighbors define the spatial clique  $\mathcal{S}$  and the two nearest neighbors in the temporal domain define the temporal clique  $\mathcal{T}$ . The choice of the potential function  $V$  is crucial to avoid blurring of edges, which in this model correspond to transitions between activated and non-activated areas in the spatial domain, resp. activated and baseline periods in the temporal domain. We have selected a  $\Phi$ -model on pairwise interactions, which presents a good behavior for edge recovery [16]:

$$\Phi(y) = \frac{-\beta}{1 + (|y|/\delta)^2}. \quad (8)$$

This function depends on two parameters,  $\beta$  and  $\delta$ . The  $\delta$  parameter defines for which intensity difference between two neighboring voxels we consider to have most probably an edge. The difference between activated and non-activated areas is the same in the spatial and temporal domain, so  $\delta_{temp} = \delta_{spat}$ . The  $\beta$  parameter reflects to the cost of an edge in the potential function. We attribute the same interaction strength to cliques in the spatial and the temporal domain. Since there are twice more neighbors in the spatial domain, we consider stronger interactions for the temporal potentials:  $\beta_{temp} = 2\beta_{spat} = \beta$ , i.e.

$$\begin{aligned} V_T(y_{i,j}(t), y_{i,j}(t+1)) &= \frac{-2\beta}{1 + (y_{i,j}(t) - y_{i,j}(t+1))^2/\delta^2}, \\ V_S(y_{i,j}(t), y_{i,j+1}(t)) &= \frac{-\beta}{1 + (y_{i,j}(t) - y_{i,j+1}(t))^2/\delta^2}, \quad (9) \end{aligned}$$

where  $V_T$  denotes the temporal interaction potential and  $V_S$  the spatial interaction potential between two voxels. We also consider a  $\Phi$ -model for the data attachment term  $P(X|Y)$  and a potential  $V_D$ :

$$P(X|Y) = \frac{1}{Z} \exp[-V_D(y_{(i,j)}(t))], \quad (10)$$

$$V_D(y_{(i,j)}(t)) = \frac{-\beta_D}{1 + (y_{(i,j)}(t) - x_{(i,j)}(t))^2/\delta^2}, \quad (11)$$

which attaches the restored signal  $Y$  to the measured data  $X$ . Using eqn. 6, 7 and 10, the *a posteriori* probability  $P(Y|X)$  is written as follows:

$$\begin{aligned} P(Y|X) &\propto P(X|Y)P(Y) \\ &\propto \prod_{(i,j),t} p(x_{(i,j)}(t)|y_{(i,j)}(t)) \exp[-U(Y)] \\ &\propto \exp[-\sum_{(i,j),t} \log p(x_{(i,j)}(t)|y_{(i,j)}(t))] \exp[-U(Y)] \\ &\propto \exp[-U_X(Y)] \quad (12) \end{aligned}$$

where the energy  $U_X$  is defined using the potentials defined in eqn. 9 and 11:

$$\begin{aligned} U_X(Y) &= \sum_{(i,j),t} V_L(y_{(i,j)}(t)) + \sum_{c \in \mathcal{T}} \sum_{(i,j)} V_T(c) + \\ &\quad \sum_{c \in \mathcal{S}} \sum_t V_S(c) \quad (13) \end{aligned}$$

The global energy is defined up to an additive constant, so we can impose  $\beta_D = 1$  without loss of generality. Thus, the proposed model depends only on the parameters  $\beta$  and  $\delta$ .

To find the configuration which minimizes the global energy corresponding to the MAP criterion, we apply a simulated annealing scheme [3]. In a parameter study of this scheme, we have selected a starting temperature of  $T = 20000$ , a temperature decrease of  $\Delta = 0.97$ , and 500 iterations.

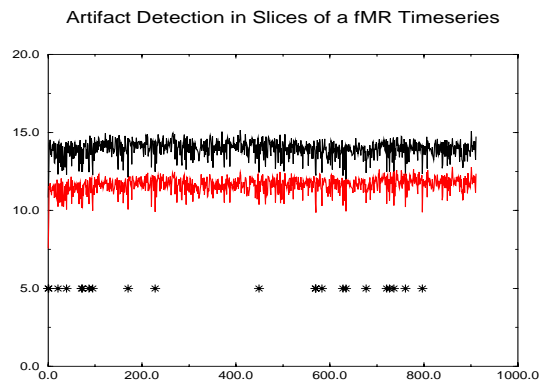


**Figure 2. Artifact detection in slices of a fMR time series. Top row: quotient of foreground and background intensity; bottom row: quotient of foreground and background variance. Stars denote slices marked as statistical outliers.**

### 3.5. Detection of Activated Areas

Data preprocessing is followed by a statistical analysis to detect signal changes that are correlated significantly with the experimental design. Usually, we compute the Pearson correlation coefficient with a box-car-waveform [6], which is shifted by 6s to take the lag of the hemodynamic response into account. The correlation coefficient is renormalized and converted into a z-statistic [23]. Activated areas are then tested for their significance using the theory of excursion sets in Gaussian random fields [14].

## 4. Results

In the context of a fMR study of auditory language comprehension we have acquired every 2s 4 slices of 128x64 voxel with a spatial resolution of 1.9x3.8x5mm and 2mm gap. The presentation of a sentence needed approx. 6s (3 timesteps), followed by a pause of 18s (9 timesteps). 76 trials (912 timesteps) were recorded during an approx. 30min experiment. A single dataset was chosen to demonstrate the use of the procedures discussed in this article. Similar evaluations have been performed on a large number of datasets and different experimental designs.

### 4.1. Artifact Detection

Fig. 2 shows a typical output of the artifact detection routine. The quotient of the foreground and background intensity (top row) shows some spikes to lower values. At these time points visual inspection mostly shows that these slices are blurred due to gross movement artifacts.

### 4.2. Movement Correction

As explained earlier, we currently perform movement correction in 2D only. Typical deviations for the time series of an axial slice are in the order of  $\pm 0.5$  mm and somewhat higher for the x (ear to ear) than for the y (front to back) direction. However, the highest degree of freedom is found in the nodding direction, which corresponds to a through-plane movement here and is currently uncorrected.

### 4.3. Baseline Correction and Signal Restoration

We selected the time series of a single voxel in a weakly activated area in the left thalamus (native z-score 2.54). Results are compiled in Fig. 5, where on the left side the time series, on the right side the spectrum is displayed. The top row contains the native signal, the second row the baseline-filtered signal (using a MA filter), the third row the baseline-filtered signal (using a FIR lowpass filter), the bottom row the bandpass-filtered signal. The native signal (top left) contains rather large baseline fluctuations ( $\sim 700$  intensity units), compared to a peak functional signal of about 80 intensity units. By bandpass-filtering a clear separation of individual trials from noise and artifacts is achieved and reflected as a prominent peak in the spectrum (at  $x = 76$ ), an impressive increase in the signal-to-noise ratio (SN) and the Pearson correlation coefficient (R) with a box-car-waveform. It is important to design the baseline filter not to diminish the first harmonic of the hemodynamic response, which is reflected in similar SN ratios of the native and filtered signals. Empirically, we found an optimum value of  $\lambda$  (in eqn. 3) of 1.5 times the period length of the intertrial interval (i.e. 18 timesteps in this example) using a filter length of  $N = 25$  coefficients.

Surprisingly, ARMA( $p, q$ ) filters do not perform better for the baseline estimation. As a performance measure, we have computed the correlation coefficient  $R$  as a function of the model coefficients  $p$  and  $q$ . Local maxima are found at ARMA(0, 18) which corresponds to a simple MA filter of length 18, and at ARMA(9, 0), which corresponds to a 9 parameter autoregressive model. A simple explanation for this finding is that ARMA models adapt to the time course too closely and follow the functional activation in the estimated baseline. Subtraction of this baseline thus diminishes (or even destroys) functional activation in the filter output. Using Akaike's information criterion to select the best model we found an ARMA(2, 2) filter.

To test the signal recovery performance of these filters, we run a second experiment. We randomly selected a non-activated voxel from a different brain region, where we expect the same artifacts and noise level. Onto this time series, we modulated (1) a square wave (in the shape of the

Waveform	square	hdr	sine
BL-MA	0.413	0.550	0.567
BL-LP	0.428	0.565	0.587
BP( $\lambda=4$ )	0.505	0.832	0.971
BP( $\lambda=3$ )	0.780	0.947	0.945
AR(9, 0)	0.536	0.738	0.773

**Table 1. Recovery rates  $c$  for model functions square wave, prototypical hemodynamic response, and sine wave. The best signal quality for the hemodynamic response is achieved using a bandpass filter which includes the first harmonic ( $\lambda = 3$ ).**

box-car-waveform), (2) a sine wave, and (3) a prototypical hemodynamic response function, which was gained by averaging over all responses in time and space in this dataset. We define the signal recovery  $c$  of the model function  $m(t)$  from the preprocessed time series  $y_s(t)$  by:

$$c = \frac{\sum_t^N (y_s(t) - (am(t) + b))^2}{\sum_t^N y_s(t)^2}, \quad (14)$$

where we maximize  $c$  by variation of  $a$  and  $b$ . Thus,  $c = 1$  denotes a perfect recovery, while  $c = 0$  corresponds to a complete loss of the signal.

Data for the various preprocessing options are collected in Tab. 1. Not surprisingly, a sine wave modulation yields the best, and a square wave the worst recovery rates. The prototypical hemodynamic response compares more with a sine wave than with a square wave, indicating the only the first harmonic is important to describe the signal shape. Surprisingly we found recovery rates of only 0.55 for baseline-filtered signals. This indicates that simple averaging the signal (in time or space) does not successfully recover the hemodynamic response. Again, bandpass-filtering yields an impressive increase, with recovery rates for the hemodynamic response of up to 0.95.

Next, we studied the performance of signal restoration using the proposed MRF. A 10x10 voxel patch was selected from the input dataset where no activation was detected and the three model functions were modulated onto this patch, convolved with a smooth 6x6 spatial kernel. We report the recovery rates under different combinations of the MRF restoration parameters  $\beta$  and  $\delta$  in Fig. 3. Higher values of  $\delta$  improve the discrimination between noise and signal, on the expense that small functional signals might be suppressed. Higher values of  $\beta$  enhance the interaction between voxels. The map-like structure of this plot stems from the fact that the simulated annealing is a stochastically driven process and yields only a solution close to the global optimum. However, consistently high values for the recovery (in the range of 0.90-0.97) are found for  $\beta > 0.3$  and  $\delta > 20$ . In

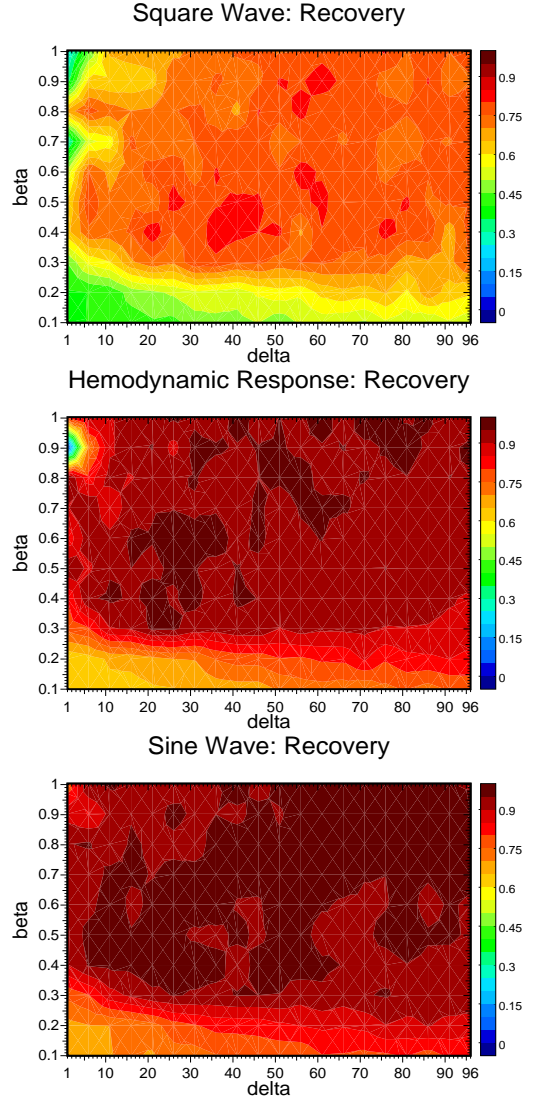


**Figure 3. fMRI signal restoration by an edge-preserving Markov random field: as a function of the restoration parameters  $\beta$  and  $\delta$ , the signal recovery for a sine wave (left), a prototypical hemodynamic response, and a square wave (right) are shown.**

conjunction with the plots for the SN ratio and the correlation (not shown) we have selected an optimum of  $\beta = 0.4$  and  $\delta = 60$ . Thus, by application of an MRF for signal restoration we yield approximately the same recovery rates (and a similar SN ratio) like in a matched bandpass filter, without having the need to infer any knowledge about the experimental design in the restoration process. To compare the edge-preserving properties of the MRF approach in comparison with spatial Gaussian filtering, we computed the performance measures SN ratio, z-score, and signal recovery for all voxels in the test patch which was modulated

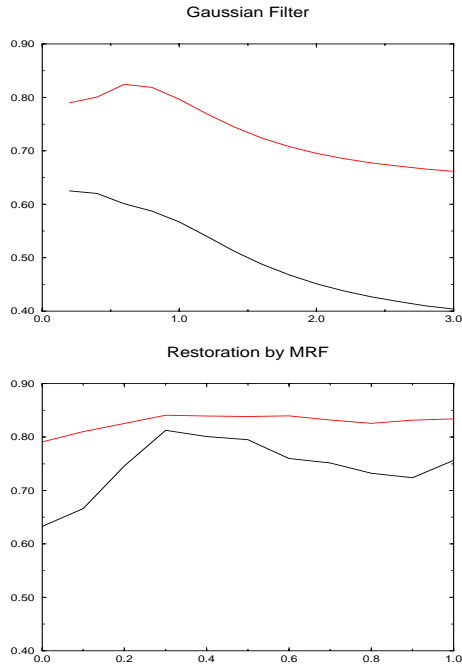


**Figure 4. Edge preservation properties of Gaussian filtering in the spatial domain (as a function of  $\sigma$ , left) in comparison with image restoration by the proposed MRF (as a function of  $\beta$ , right). The upper trace corresponds to the z-score correlation, the lower to the SN correlation. For more explanation, please refer to the text.**

with either a square wave, the hemodynamic response, or a sine wave. Then we computed the likelihood (i.e. the correlation) of these measures with the spatial convolution kernel applied in the modulation. An ideal procedure would produce a correlation of 1, and 0 would indicate a complete loss (or distortion) of the modulation. Results for the hemodynamic response are shown in Fig. 4, where the upper trace corresponds to the z-score correlations, the lower trace to the SN ratio correlations.

With an increasing  $\sigma$  of the Gaussian filter, a slight increase followed by a marked decrease of the correlation is found. This corresponds well to the "usual practice" of applying a Gaussian filter with an optimal  $\sigma$ -value of 0.6, while higher values introduce considerable blur in the statistical parameter maps. The MRF yields consistently better figures in all test measures and all types of signals (not shown).

Fig. 6 (see last page of the paper) compiles the results of the statistical analysis of this dataset. Immediately evident is the improvement in the z-statistics after bandpass filtering: in the auditory cortex, z-scores up to 20 are found. However, by filtering in the temporal domain only, varia-

tions between voxels occur. When using a MRF for signal restoration, smooth but not blurred activations are found.

## 5. Discussion

We propose a preprocessing sequence for fMR data, which consists of (1) artifact detection, (2) movement correction, (3) baseline correction, and (4) signal restoration using an edge-preserving MRF. The advantages of this sequence are reflected in impressive increases of z-scores in the test statistics and a better signal-to-noise ratio, which corresponds to a lower rate of false positively detected activations. To test the signal quality after preprocessing, we modulated test signals onto raw fMR datasets and computed their recovery. For a prototypical hemodynamic response we were able to recover up to 95% of the original signal shape, compared to 45% in the native (unprocessed) case. In contrast to Gaussian filtering in the spatial domain, the standard procedure to improve the signal-to-noise ratio of functional MR data, our signal restoration method yields a better signal recovery and introduces less blur in the spatial domain.

However, our approach has some limitations: (1) time steps marked as artifact-loaded during the first preprocessing step are reconstructed from the neighbors to allow the processing of time series in subsequent steps. This ad-hoc method needs re-evaluation. (2) it remains unclear how much the use of spatio-temporal interactions in the MRF affects test statistics. Although as far as we know, the currently accepted application of Gaussian filtering in the spatial domain, has not been studied in this context, an evaluation using Monte Carlo simulations seems necessary. (3) the MRF is computationally expensive. A typical MR experiment needs 3-4h of restoration time, compared with 5min for bandpass filtering. Thus, the use of the MRF might be deferred until the final statistical evaluation.

Two important advantages of the preprocessing scheme proposed here should also be emphasized: firstly, a reliable baseline correction makes it possible to compare experimental blocks which were recorded several minutes apart or even in different scans. Secondly, a good signal restoration renders complex schemes for hemodynamic modeling less interesting. The vast improvement in signal quality and a proven recovery of more than 90% of the original signal shape allow a better comparison of the dependency between the shape of the hemodynamic response and different cognitive stimulation conditions.

These benefits from preprocessing of fMR data open new perspectives for the design of fMR experiments in cognitive research.

**Acknowledgement-** The authors wish to thank Dr. David Norris for providing the data sets and Martin Meyer for designing and conducting the fMR experiments.

## References

- [1] H. Andrews and B. Hunt. *Digital image restoration*. Prentice Hall, Englewood Cliffs, N.J., 1977.
- [2] H. Benali, I. Buvat, J. L. Anton, M. Pelegrini, M. Di Paola, J. Bittoun, Y. Burnod, and R. Di Paola. Space-time statistical model for functional mri image sequences. *Information Processing in Medical Imaging (IPMI '97)*, Lecture Notes in Computer Science 1230, 1997.
- [3] M. Berthod, Z. Kato, S. Yu, and J. Zerubia. Bayesian image classification using markov random fields. *Image and Vision Computing*, 14:285–295, 1996.
- [4] R. B. Buxton and L. R. Frank. A model for the coupling between cerebral blood flow and oxygen metabolism during neuronal stimulation. *Journal of Cerebral Blood Flow and Metabolism*, 17:64–72, 1997.
- [5] B. Chalmond. Image restoration using an estimated Markov model. *Signal Processing*, 15:115–129, 1988.
- [6] M. S. Cohen. Parametric analysis of fmri data using linear systems methods. *Neuroimage*, 6:93–103, 1997.
- [7] H. Derin and H. Elliott. Modelling and segmentation of noisy and textured images using gibbs random fields. *IEEE Trans. on Pattern Analysis and Machine Intelligence*, 9(1):39–55, 1987.
- [8] X. Descombes. A dense class of markov random fields and associated parameter estimation. *Journal of Visual Communication and Image Representation*, 3:97, 1997.
- [9] X. Descombes, F. Kruggel, and D. Y. von Cramon. Fmri signal restoration using an edge preserving spatio-temporal markov random field. *Technical Report 12/97, MPI of Cognitive Neuroscience*, 1997.
- [10] X. Descombes, F. Kruggel, and D. Y. von Cramon. Spatio-temporal fmri analysis using markov random fields. *Technical Report 4/97, MPI of Cognitive Neuroscience*, 1997.
- [11] R. Dymond and D. Norris. Mechanism and echo time dependence of the fast response in fmri. *Magnetic Resonance in Medicine*, 38:1–6, 1997.
- [12] K. J. Friston, C. D. Frith, R. S. J. Frackowiak, and R. Turner. Characterizing dynamic brain responses with fmri: a multivariate approach. *Neuroimage*, 2:166–172, 1995.
- [13] K. J. Friston, S. Williams, R. Howard, R. S. J. Frackowiak, and R. Turner. Movement-related effects in fmri timeseries. *Magnetic Resonance in Medicine*, 35:346–355, 1996.
- [14] K. J. Friston, K. J. Worsley, R. S. J. Frackowiak, J. C. Mazziotta, and A. C. Evans. Assessing the significance of focal activations using their spatial extent. *Human Brain Mapping*, 1:210–220, 1994.
- [15] S. Geman and D. Geman. Stochastic relaxation, gibbs distributions, and the bayesian restoration of images. *IEEE Transactions on Pattern Analysis and Machine Intelligence*, 6:721–741, 1984.
- [16] S. Geman and G. Reynolds. Constrained restoration and recovery of discontinuities. *IEEE Transactions on Pattern Analysis and Machine Intelligence*, 14(3):367–383, 1992.
- [17] X. Hu and S. G. Kim. Reduction of signal fluctuation in functional mri using navigator echoes. *Magnetic Resonance in Medical Imaging*, 31:495–503, 1994.
- [18] N. Lange. Tutorial in biostatistics: statistical approaches to human brain mapping by functional magnetic resonance imaging. *Statistics in Medicine*, 15:389–428, 1996.
- [19] N. Lange and S. L. Zeger. Non-linear fourier time series analysis for human brain mapping by functional magnetic resonance imaging. *Journal of Royal Statistical Society, Applied Statistics*, 46(1):1–29, 1997.
- [20] M. McKeown, T. P. Jung, S. Makeig, G. Brown, S. S. Kindermann, T. W. Lee, and T. J. Sejnowski. Spatially independent activity patterns in functional mri data during the stroop color naming task. *Proceedings of the National Academy of Science USA*, in print, 1998.
- [21] D. C. Noll, C. R. Genovese, A. L. Vazques, and W. Eddy. Evaluation of respiratory artifact correction techniques in fmri using roc analysis. *Proceedings of 4th Meeting of the International Society of Magnetic Resonance*, page 343, 1996.
- [22] J. B. Poline and B. M. Mazoyer. Enhanced detection in brain activation maps using a multifiltering approach. *Journal of Cerebral Blood Flow and Metabolism*, 14:639–642, 1994.
- [23] W. H. Press, S. A. Teukolsky, W. T. Vetterling, and B. P. Flannery. *Numerical Recipes in C*. Cambridge University Press, Cambridge, MA, 1992.
- [24] J. C. Rajapakse and F. Kruggel. Neuronal and hemodynamic responses from functional mri timeseries: a computational model. *Proceedings of International Conference on Neural Information Processing*, Christchurch, New Zealand, 1997.
- [25] J. C. Rajapakse, F. Kruggel, J. Maisog, and D. Y. von Cramon. Modeling hemodynamic response for analysis of functional mri timeseries. *Human Brain Mapping*, in print, 1998.
- [26] C. B. Rorabaugh. *Digital filter designer's handbook*. McGraw Hill, New York, NY, 1993.
- [27] G. Scarth, M. Alexander, M. McIntyre, B. Wowk, and R. L. Somorjai. Artifact detection in fmri using fuzzy clustering. *Proceedings of 4th Meeting of the International Society of Magnetic Resonance*, page 1783, 1996.
- [28] J. A. Sorenson and X. Wang. Problems in estimation hemodynamic response parameters from fmri data. *Human Brain Mapping*, 4:265–272, 1998.
- [29] A. Villringer and U. Dirnagl. Coupling of brain activity and cerebral blood flow: basis of functional imaging. *Cerebrovascular and Brain Metabolism Review*, 7:240–276, 1995.
- [30] M. West and J. Harrison. *Bayesian forecasting and dynamic models*. Springer Verlag, Heidelberg, 1997.

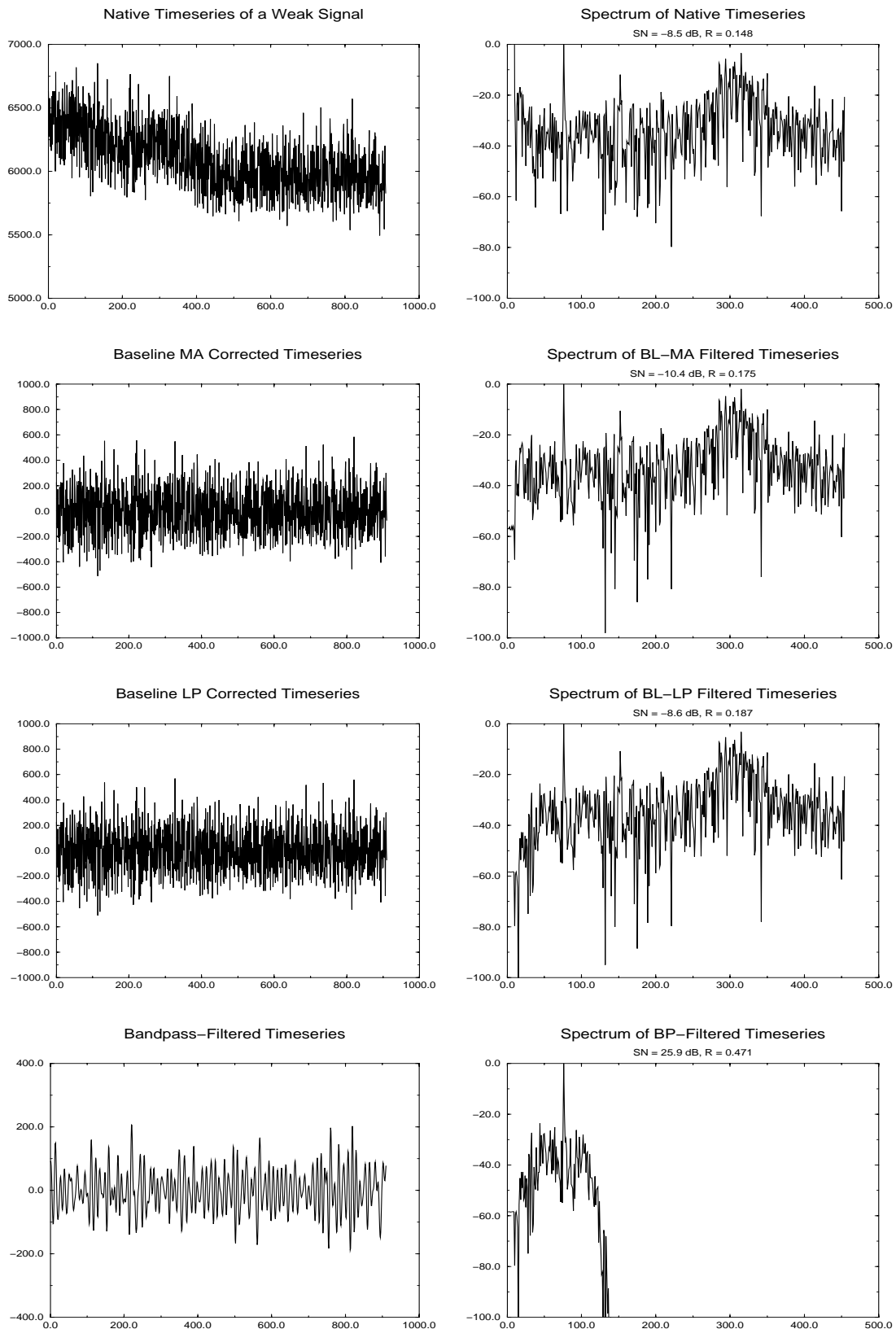


**Figure 5. Timeseries (left) and spectra (right) at a voxel with low activation. Top row: native signal, 2nd row: after baseline correction using an MA filter, 3rd row: after baseline correction using an LP filter, bottom row: after BP filtering. Listed with the spectra are the signal-to-noise ratio (SN) and the Pearson correlation (R) coefficient with the stimulus, modeled as a box-car-waveform.**

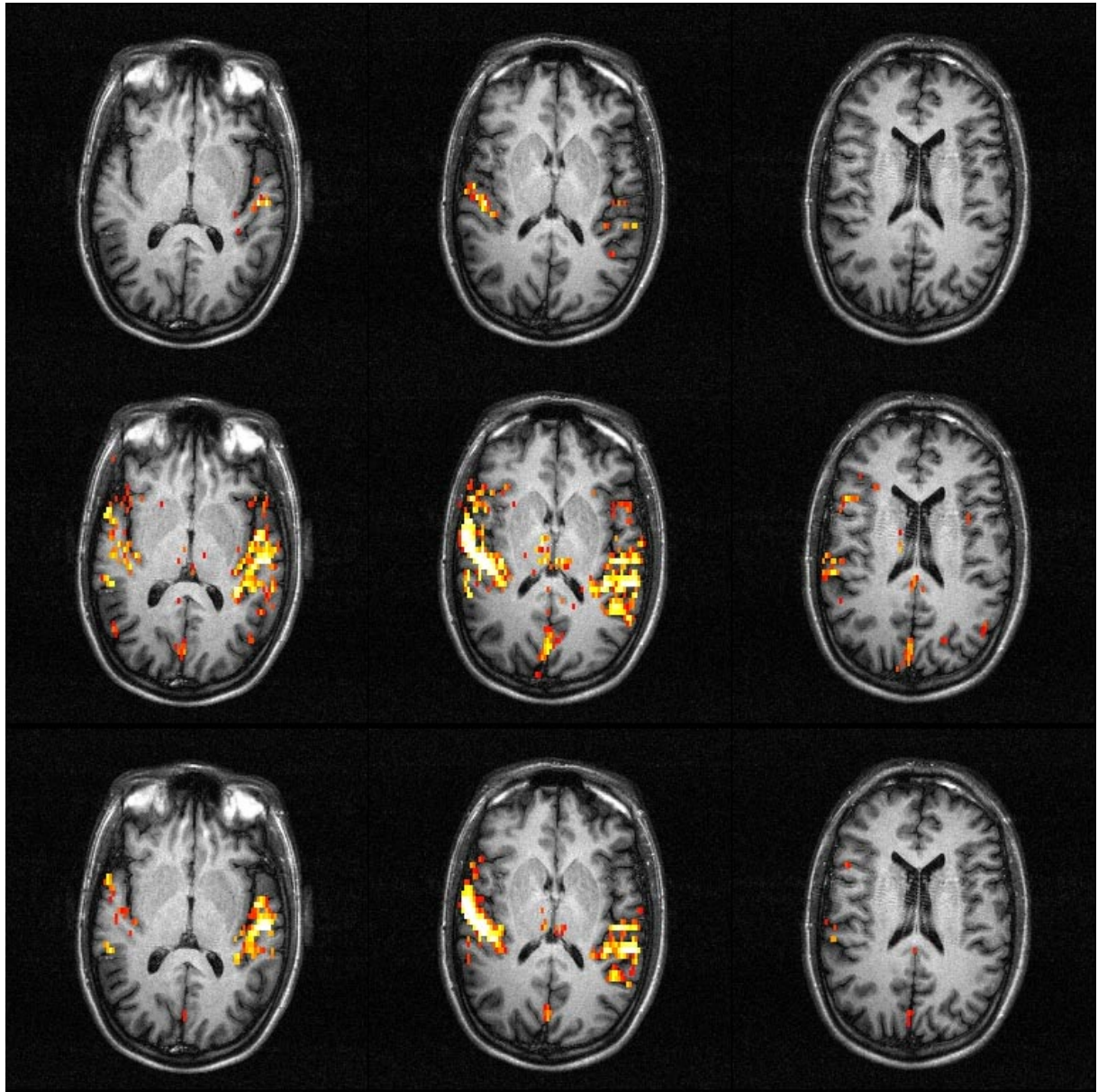


Figure 6. Statistical analysis of a fMR experiment to study auditory language processing. Top row: analysis of the native dataset, middle row: after bandpass filtering, bottom row: after image restoration using an MRF. For the detection of activated regions we have computed the Pearson correlation coefficient with a box-car-waveform (shifted by 6s), followed by z-transformation and assessment for significance. The "hot body" color scale ranges from  $z = 12$  (!) to 24.